Jurnal Polimesin
Department of Mechanical Engineering
State Polytechnic of Lhokseumawe
http://e-jurnal.pnl.ac.id/polimesin
e-ISSN : 2549-1999 No. : 2 Month : April
p-ISSN : 1693-5462 Volume : 24 Year : 2026

Processing dates: received on 2025-9-27, reviewed on 2026-03-01, accepted on 2026-03-03 and online availability on 2026-04-27

Thermal distribution and macrostructural characteristics of TIG-welded Cu/SS316L dissimilar joints: experimental and numerical study

Azwinur[1,2], Agus Suprihanto[1], Mukhsinun Hadi Kusuma[3*], Khoiri Rozi[1], Usman[2], Surya Dharma[4], Hamdani[2]
[1]Department of Mechanical Engineering, Diponegoro University, Semarang 50275, Indonesia
[2]Department of Mechanical Engineering, Politeknik Negeri Lhokseumawe, Lhokseumawe 24301, Indonesia
[3]Research Center for Nuclear Reactor Technology, Research Organization for Nuclear Energy, National Research and Innovation Agency, Tangerang Selatan 15314, Indonesia
[4]Department of Mechanical Engineering, Politeknik Negeri Medan, Medan 20155, Indonesia
*Corresponding author: mhad001@brin.go.id

Abstract

Dissimilar welding of copper (Cu) and Stainless Steel 316L (SS316L) presents significant challenges due to their large differences in thermal conductivity and melting temperature, which lead to asymmetric heat distribution and non-uniform penetration. This study aims to evaluate the effect of welding current on temperature distribution and macrostructural characteristics of TIG-welded Cu/SS316L joints using ERCuSi-A filler through an integrated experimental and numerical approach. Welding experiments were conducted at three current levels: 120 A, 135 A, and 150 A on 2.7 mm thick plates. Macrostructural examinations were performed to assess weld bead geometry and penetration behavior. Transient thermal simulations were carried out using ANSYS Workbench to predict temperature fields and thermal gradients. The results indicate that welding current significantly influences weld morphology and thermal behavior. At 120 A, the weld bead was relatively narrow with limited penetration on the Cu side due to rapid heat dissipation. At 135 A, a more uniform fusion profile was achieved, with simulated peak temperatures exceeding 1000°C and an improved penetration balance between Cu and SS316L. At 150 A, deeper penetration into SS316L was observed; however, the heating cycle became shorter and the temperature distribution more localized. Numerical results consistently showed asymmetric temperature fields, where heat diffused rapidly into Cu and concentrated in SS316L. The strong correlation between simulation and macrostructural observations confirms that thermal distribution governs weld geometry and penetration behavior. The 135 A current provides the most balanced fusion characteristics, making it suitable for Cu/SS316L dissimilar joints in heat-transfer applications.

Keywords:
Cu/SS316L, TIG welding, ANSYS simulation, temperature distribution, macrostructural analysis, dissimilar metal welding.

1 Introduction

Welding is one of the most widely applied joining technologies in modern manufacturing industries. The process is based on the partial melting of base metals with or without the addition of filler metal, followed by solidification to form a metallurgical bond [1]. Compared to other joining methods, such as brazing or mechanical fastening, welding offers efficiency, high joint strength, and the ability to fabricate complex components on an industrial scale. For this reason, welding technology has become a fundamental pillar in the fabrication of steel structures, shipbuilding, power plants, petrochemical facilities, and nuclear energy systems [2].

The properties of welded joints are strongly influenced by the characteristics of the materials being welded, process parameters, and the mechanism of heat transfer during welding [3][4]. In similar metal welding, parameter control is relatively straightforward because the physical and metallurgical properties of the materials are compatible. However, in dissimilar metal welding, significant differences in thermal conductivity, melting temperature, and coefficient of thermal expansion often result in non-uniform heat distribution, asymmetric penetration, and a higher tendency for metallurgical defects such as cracks, porosity, and lack of fusion [5][6].

Among the various combinations of dissimilar metals, copper (Cu) and austenitic Stainless Steel 316L (SS316L) are frequently considered for applications in cooling systems. Copper exhibits very high thermal conductivity (~390 W/m·K), a relatively low melting point (1085°C), and a high thermal expansion coefficient, which causes heat from the arc to dissipate rapidly and makes it difficult to maintain a stable molten pool during welding [7][8]. In contrast, SS316L possesses much lower thermal conductivity (~16 W/m·K), excellent corrosion resistance, and stable mechanical strength at medium to high temperatures [9]. These contrasting properties make the Cu–SS316L joint highly attractive to weld because it can provide a unique combination of copper's high thermal conductivity and stainless steel's corrosion resistance. However, these differences also lead to the formation of brittle phases, non-uniform fusion, and residual stresses, which inherently make the welding process more challenging [6][10].

Among the various welding processes, Tungsten Inert Gas (TIG) welding, also known as Gas Tungsten Arc Welding (GTAW) [11], is considered the most suitable for Cu–SS316L joining [11][12]. TIG welding employs a non-consumable tungsten electrode to generate an electric arc, while the filler rod is added separately. The process is renowned for producing high-quality joints due to its arc stability and effective inert gas protection. The shielding gas, commonly pure argon, prevents oxidation of both the molten pool and tungsten electrode, while backing gas is supplied to the reverse side of the joint to protect the root from atmospheric contamination [13][14]. Direct Current with the Electrode Negative (DCEN) is generally preferred, as it promotes deeper penetration and greater electrode stability. However, welding current must be carefully selected, since it governs the heat input, which in turn controls penetration and thermal distribution [15].

Heat input represents the total thermal energy delivered to the material during welding and is primarily influenced by welding current, arc voltage, and welding speed. In dissimilar metal welding such as Cu–SS316L, the control of heat input becomes particularly critical due to the significant mismatch in thermophysical properties between the two materials.

The welded Cu/SS316L configuration combines the superior thermal conductivity of copper with the corrosion resistance and structural strength of stainless steel, creating a material system that is highly suitable for applications demanding efficient heat transfer along with electrochemical stability. Despite these advantages, joining these two dissimilar materials introduces significant thermo-metallurgical complexities due to the pronounced differences in their physical properties [16]. The substantial gap in melting temperature [17], thermal conductivity [18], and coefficient of linear expansion [19] promotes the formation of sharp thermal gradients during the welding process, which significantly influence heat flow and solidification behavior.

These differences significantly affect heat flow behavior, molten pool stability, and solidification dynamics. Excessive heat input may result in excessive melting on the stainless steel side, enlargement of the Heat-Affected Zone (HAZ), and increased

distortion, whereas insufficient heat input may cause shallow penetration on the copper side and potential lack of fusion at the interface. Therefore, optimizing welding current through controlled heat input is essential to achieve balanced thermal distribution, stable fusion geometry, and reliable joint integrity in Cu/SS316L dissimilar welding.

In addition to process parameters, the choice of filler rod plays a decisive role in the success of Cu–SS316L welding [20][21]. The filler not only acts as the bridging medium but also controls the chemical composition of the fusion zone to stabilize the transition between Cu and SS316L. Direct interaction between copper and iron often leads to the formation of brittle intermetallic compounds, so the presence of certain alloying elements in the filler becomes critical to improve metallurgical compatibility. Elements such as silicon, nickel, and deoxidizers can enhance fluidity, reduce oxidation, and improve the homogeneity of the mixed zone. Hence, the synergy between filler chemistry and the thermal characteristics of Cu and SS316L is one of the key factors determining the integrity of the joint.

From a metallurgical perspective, macrostructural analysis of weld cross-sections is a fundamental characterization method to evaluate joint quality. Macro examination reveals fusion geometry, penetration depth, weld bead width, and the extent of the HAZ, providing essential information on weld homogeneity and the presence of macroscopic defects. Without macrostructural analysis, numerical modeling of thermal distribution remains predictive only and cannot be experimentally validated.

Alongside experimental approaches, numerical simulation has become an indispensable tool for understanding the welding process [22]. Finite Element Analysis (FEA) using software such as ANSYS enables the prediction of thermal distribution, temperature gradients, and heat flow during welding [23], [24]. The present transient thermal model adopts similar Finite Element Method (FEM) based approaches reported in previous welding simulation studies [22], [23], [24], [25], including Gaussian heat source representation and refined meshing near the weld path, to ensure methodological consistency and validation reliability.

In this context, the present study integrates numerical and experimental approaches to investigate TIG welding of Cu–SS316L joints with a filler metal that is chemically compatible with both materials. Thermal distribution is analyzed using ANSYS simulation, while weld macrostructure is evaluated experimentally through macrostructural examination. The novelty of this work lies in the systematic correlation between numerically predicted thermal fields and experimentally validated macrostructural features, which has rarely been reported for Cu–SS316L dissimilar joints. This approach is expected to strengthen the understanding of the interrelationship between thermal phenomena, filler role, and macrostructural morphology, thereby contributing to the development of optimized dissimilar welding strategies for energy systems and high-performance cooling applications.

2 Materials and experimental methods

2.1 Materials

The base materials used in this study were commercially available copper (Cu) plates and austenitic SS316L plates, each with a thickness of 2.7 mm. The plates were cut into rectangular specimens and arranged in a butt joint configuration for welding. The primary focus of the experimental characterization was on the welded joints formed between copper (Cu) and SS316L. Before welding, the plate surfaces were mechanically ground and cleaned with acetone to remove oxides and surface contaminants, ensuring good metallurgical bonding.

2.2 Welding procedure

Welding was performed using the TIG process, also known as GTAW. This process was selected because of its ability to produce high-quality joints, stable arc control, and effective inert gas shielding. A non-consumable tungsten electrode was used to generate the arc, while filler rods of type ERCuSi-A were manually added into the molten pool. The ERCuSi-A filler was chosen because its silicon content improves wetting on copper surfaces, reduces oxidation, and enhances metallurgical compatibility at the Cu–SS316L interface, thereby reducing the tendency for brittle intermetallic formation and promoting a more homogeneous fusion zone.

Pure argon (99.99%) was used as the shielding gas at a controlled flow rate to protect both the molten pool and tungsten electrode from oxidation. Additionally, argon was supplied as a backing gas on the root side of the joint, primarily to protect the stainless steel region from oxidation during welding. The welding polarity was DCEN.

Welds were produced at three different current levels: 120 A, 135 A, and 150 A. These current variations were intentionally selected to generate different levels of heat input during the welding process. Since welding current directly determines the amount of thermal energy delivered to the arc, an increase in current results in higher heat input to the material when other parameters remain constant.

The corresponding heat input values for each current level are presented in Table 1. Variations in heat input significantly influence penetration depth, fusion zone geometry, thermal gradients, and the width of the HAZ. Therefore, controlling welding current is essential for achieving balanced thermal distribution and stable weld morphology in Cu/SS316L dissimilar joints.

Table 1. Welding parameter

Sample (No.)	Welding current (A)	Volt (V)	Welding speed (mm/min)	Welding heat Input (kJ/mm)
1#	120	12	42.79	2.02
2#	135	12	47.61	2.04
3#	150	12	76.69	1.41

2.3 Sample preparation for macrostructural examination

After welding, the joints were sectioned perpendicular to the weld bead to obtain transverse cross-sections. The specimens were prepared for macrostructural analysis by successive grinding using silicon carbide abrasive papers of 240, 400, 600, and 1200 grit, followed by polishing with velvet cloth and alumina suspension. The polished surfaces were etched with suitable chemical reagents to clearly reveal the weld morphology, including the fusion zone, HAZ, and base metals.

Macrostructural examination was carried out using an optical digital microscope. The features analyzed included fusion geometry, penetration depth, weld bead width, and the extent of the HAZ. These results were used to assess weld quality and to validate the numerical predictions of thermal distribution.

2.4 Numerical simulation

Numerical simulations of the welding process were conducted using the FEM in ANSYS Workbench. A three-dimensional model of the Cu–SS316L butt joint was developed, and the thermal properties of each base metal were assigned according to literature values. The heat source was modeled using a Gaussian distribution to represent the TIG arc, with parameters corresponding to the three current levels.

The simulations were performed under transient thermal conditions to replicate the heating and cooling cycles of welding. Boundary conditions included convective and radiative heat losses to the surroundings, while the initial plate temperature was set to match experimental conditions. The mesh was refined in the weld region to capture steep temperature gradients.

The simulation results, including temperature distribution maps, isothermal profiles, and thermal gradients, were compared with experimental macrographs to evaluate the consistency between numerical predictions and actual weld morphology. This integrative

approach enabled a systematic understanding of the relationship between heat distribution and macrostructural features in TIG-welded Cu/SS316L joints.

3 Results and discussion

3.1 Experimental weld morphology

The results of the welding experiments are presented in Fig. 1, which shows the macrostructural appearance of the Cu/SS316L joints produced by the TIG welding process. The Fig. 1 illustrates the overall fusion profile, weld bead geometry, and penetration behavior at the interface between copper and stainless steel. These features provide the first indication of how thermal distribution during welding influences the formation of the weld joint. A detailed examination of the macrographs allows the identification of fusion characteristics, the extent of the HAZ, and possible asymmetry in penetration, which are directly correlated with the thermal gradients predicted by the numerical simulations.

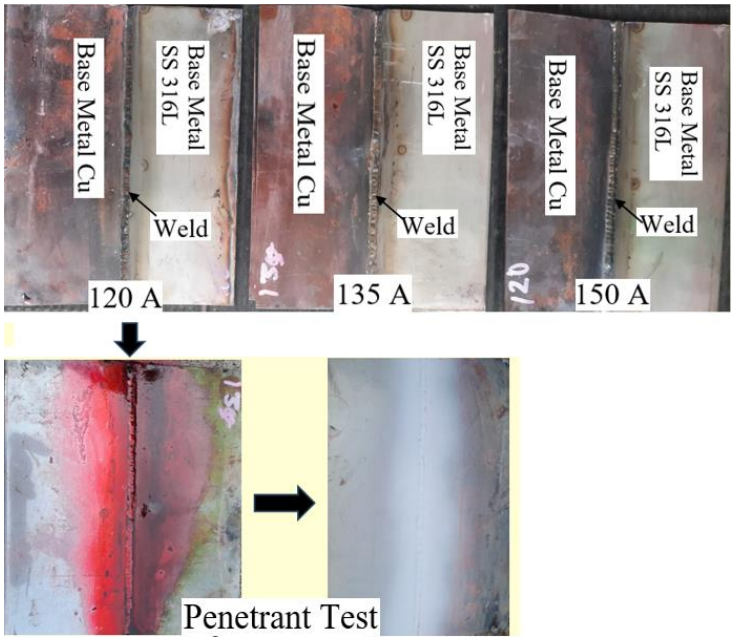

Fig. 1. Welding experiments.

Fig. 1 presents the macrostructural appearance of the Cu/SS316L welds produced using TIG welding with welding currents of 120 A, 135 A, and 150 A. At 120 A, the weld bead appears relatively narrow, reflecting the lower heat input that produces a smaller molten pool and shallower penetration, particularly on the copper side where heat is rapidly dissipated due to its high thermal conductivity. At 135 A, the bead becomes wider, and the fusion zone appears more uniform, indicating that the higher heat input promotes a more stable molten pool and improved penetration toward the SS316L side. At 150 A, the weld bead is visibly larger and the penetration deeper, especially into the stainless steel region, where the lower thermal conductivity allows heat to concentrate. However, this condition is also associated with the formation of a wider heat-affected zone, which may increase the risk of distortion or thermal defects.

The bottom part of Fig. 1 shows the results of liquid penetrant testing carried out to evaluate the surface integrity of the welds. The application of the red penetrant highlights possible surface-breaking defects such as cracks or open porosity. After cleaning, no significant defect indications were observed along the weld surface, confirming that the welds produced under these conditions were free from detectable surface cracks.

Overall, the variation in welding current strongly influences the morphology of the Cu/SS316L welds. Lower current produces insufficient penetration due to rapid heat dissipation in copper. In comparison, higher current provides deeper penetration and wider beads but increases the thermal impact on the stainless steel side. The penetrant test results further demonstrate that all welds exhibited acceptable surface quality, thereby validating the integrity of the joints at the macroscopic level.

3.2 Macrostructural observation

To obtain a more comprehensive understanding of the fusion profile and penetration characteristics of the dissimilar joint, macrostructural examinations were performed [26]. The corresponding results are presented in Fig. 2.

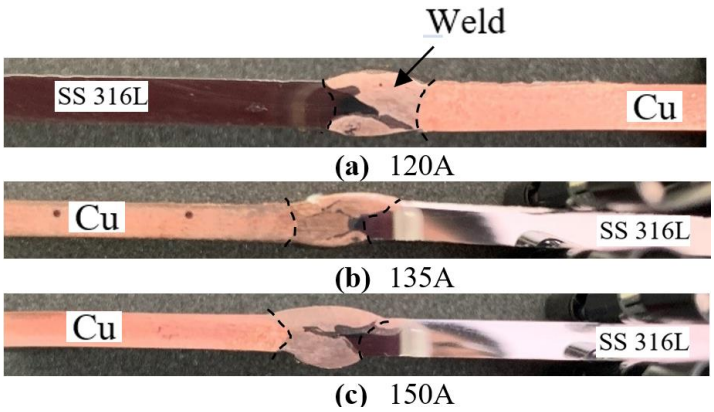

Fig. 2. Macro test.

In Fig. 2, the weld region highlighted by the dashed boundaries shows distinct morphological and color variations for the three current levels (120 A, 135 A, and 150 A) in the TIG welding of Cu–SS316L using ERCuSi-A filler metal.

Fig. 2(a), the weld bead appears relatively wider with a smoother contour and good continuity with both base metals. Within the weld zone, two dominant color tones can be observed: a reddish region and a darker grayish region. The reddish tone is likely associated with the dominance of Cu, originating from both the ERCuSi-A filler and the Cu base metal. The darker region may indicate areas enriched with Fe, Cr, and Ni, resulting from dilution of SS316L into the molten pool. The relatively smooth transition between these color regions suggests a fairly uniform metallurgical mixing in the weld center.

Fig. 2(b), the weld becomes more concentrated in the central region, and the darker zone appears more pronounced compared to 120 A. The increased contrast indicates a stronger local interaction between the filler metal and the SS316L base metal. The darker central region likely corresponds to a higher fraction of Fe-rich material due to increased melting and dilution from the stainless steel side. Meanwhile, the lighter reddish regions remain associated with Cu-dominant areas. The sharper compositional contrast suggests a more heterogeneous distribution within the weld metal.

Fig. 2(c), the weld bead appears more localized and narrower, with a more clearly defined central dark region. The darker elongated area in the center likely represents regions with higher Fe–Cr–Ni content resulting from intensified melting of the SS316L and localized mixing in the molten pool. The surrounding lighter regions remain Cu-rich. The stronger color contrast at this current level indicates a more significant compositional gradient within the weld metal, which may be associated with faster solidification and concentrated mixing behavior.

Overall, the reddish zones within the weld are predominantly associated with Cu-rich regions, while the darker gray regions are likely enriched with Fe, Cr, and Ni originating from SS316L dilution. As the welding current increases from 120 A to 150 A, the central darker region becomes more concentrated and distinct, suggesting increased localized mixing and compositional variation within the weld metal. These differences may influence the resulting microstructure and mechanical properties of the dissimilar Cu–SS316L joint.

3.3 Numerical modeling and thermal simulation

Understanding the temperature distribution is crucial, as it forms the basis for predicting the behavior of the joint during

welding. The temperature not only determines the penetration depth and fusion zone geometry but also influences the cooling rate, the potential formation of brittle Fe–Cu intermetallics, and the magnitude of residual stresses and distortion. Without knowledge of the underlying thermal distribution, optimization of welding parameters would rely solely on trial-and-error and risk producing unreliable joints. Therefore, the integration of macrostructural analysis with numerical predictions provides a strong scientific foundation for designing more reliable welding parameters for Cu–SS316L dissimilar joints.

Fig. 3(a) illustrates the geometric model used to represent the butt joint between Cu and SS316L plates with a weld length of approximately 100 mm, consistent with the simulated TIG welding configuration. The color difference in the model indicates two materials with distinct thermal properties, where Cu possesses significantly higher thermal conductivity than SS316L. Physically, this difference leads to a non-symmetric temperature distribution during the heating process. In the cross-sectional view, a groove is observed at the joint region, which serves as the path for the moving heat source.

Fig. 3(b) presents the finite element mesh configuration, showing significant mesh refinement along the weld line and around the fusion zone, while the regions farther from the heat source are modeled with a coarser mesh. This strategy is appropriate because the highest thermal gradients occur near the moving heat source; therefore, a finer mesh is required to improve the accuracy of maximum temperature prediction and thermal distribution during transient analysis.

To evaluate the temperature distribution during the welding process for sample 1# at a welding current of 120 A, a numerical simulation was performed as shown in Fig. 4 and Fig. 5. In Fig. 4(a), the temperature distribution at t = 100 s—representing the system temperature at the 100th second of the transient simulation—shows that the maximum temperature zone remains concentrated along the weld path. The red contour indicates the region with the highest temperature, corresponding to the position of the moving heat source at that moment. At a welding current of 120 A, the supplied energy is sufficient to generate a relatively wide heated region around the joint, suggesting that the fusion zone and HAZ develop significantly. The difference in thermal properties between Cu and SS316L results in a non-symmetric temperature distribution, where the SS316L side exhibits a steeper thermal gradient compared to the Cu side.

Meanwhile, the temperature distribution shown in Fig. 4(b) represents the thermal condition at the end of welding (200 s), corresponding to the final stage of the transient simulation. At this stage, heat has spread over a wider area of the plate, and the maximum temperature intensity has decreased due to natural cooling. The thermal trace along the weld line remains clearly visible, indicating that this region previously experienced significant high-temperature exposure. The temperature spread appears more pronounced on the Cu side than on the SS316L side, which is associated with the higher thermal conductivity of Cu, allowing heat to diffuse more rapidly into this material.

Fig. 5 illustrates the temperature response at three different locations: weld metal, HAZ Cu, and HAZ SS316L. The weld metal curve exhibits the highest temperature among the three regions, with a peak approaching approximately ±1050°C. This is expected, as the weld metal receives heat energy directly from the heat source. The HAZ Cu curve lies slightly below that of the weld metal but tends to be higher than the HAZ SS316L during the initial temperature rise. This indicates that the Cu side responds more rapidly to heating, which is consistent with its higher thermal conductivity, allowing heat to be distributed more quickly.

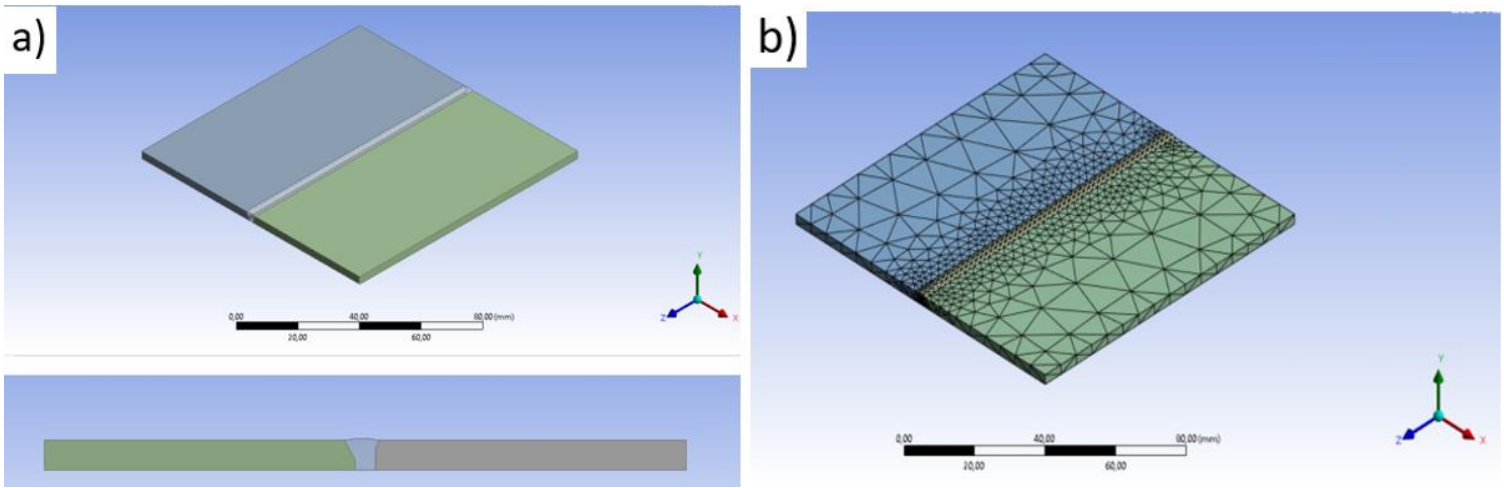

Fig. 3. (a) Geometric model of the Cu–SS316L butt joint for transient thermal simulation. (b) Finite element mesh distribution with refinement along the weld path.

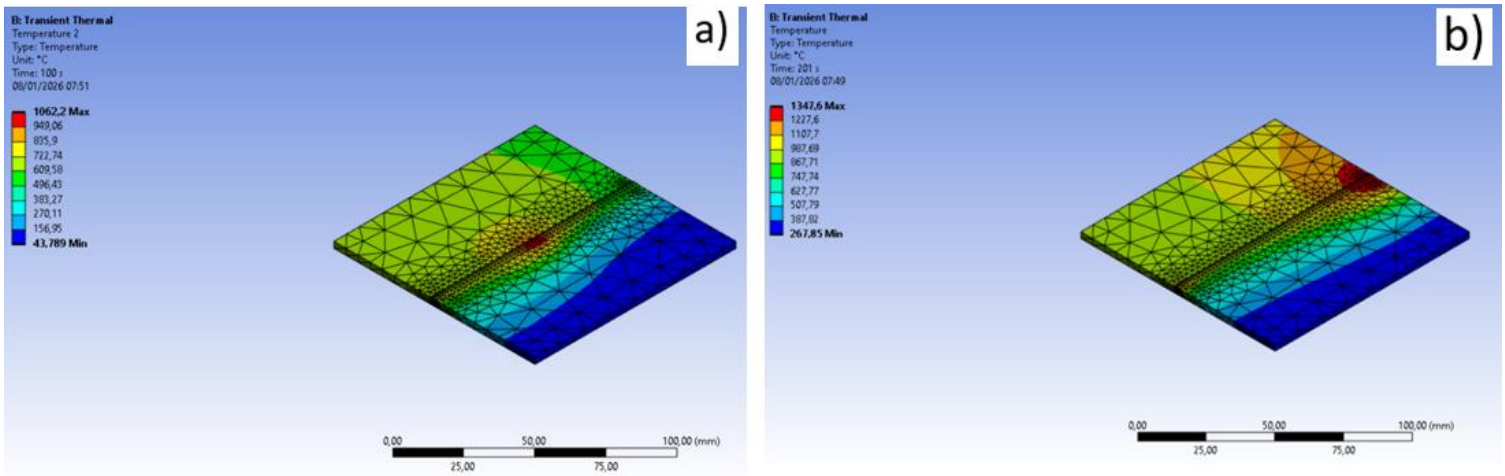

Fig. 4. (a) Temperature distribution at t = 100 s. (b) Temperature distribution at the end of welding (200 s).

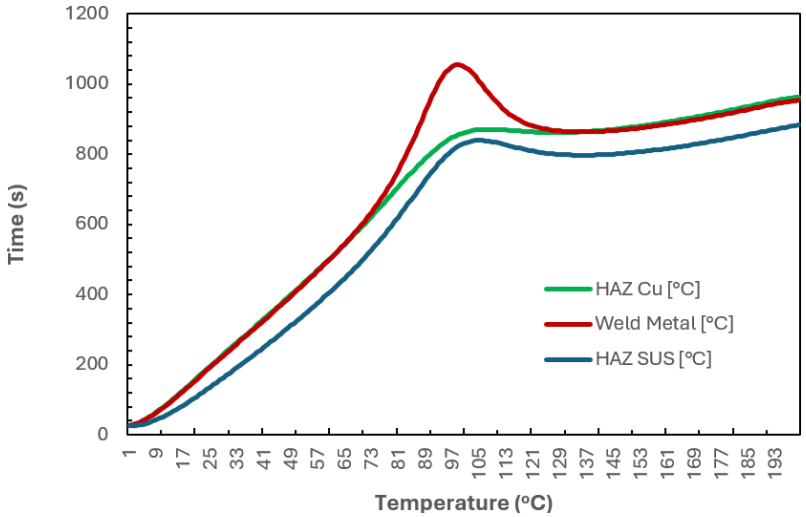

Fig. 5. Temperature distribution at the weld metal, Cu HAZ, and SS316L HAZ (120 A).

In contrast, the HAZ SS316L curve shows slightly lower temperatures and a slower thermal response compared to the Cu side. This reflects the lower thermal conductivity of SS316L, resulting in more localized heat concentration near the joint region.

After reaching their peak values, all three curves exhibit a decreasing or stabilizing trend, representing the cooling phase as the moving heat source travels away from the observation point.

The temperature distribution during the welding process for sample 2# at a welding current of 135 A was simulated as shown in Fig. 6 and Fig. 7.

Fig. 6(a) presents the temperature distribution at t = 100 s for sample 2#, where the high-temperature zone remains concentrated along the weld path, with the temperature peak located near the position of the moving heat source. Compared to sample 1#, the temperature distribution at a welding current of 135 A appears slightly more localized and less extensive than at 120 A. The red contour indicates that the maximum temperature remains above 1000°C; however, the thermal gradient around the weld line appears somewhat steeper.

This difference suggests that although the welding current increases to 135 A, the heat spread is not wider than in case 1. Instead, the heat distribution becomes more concentrated along the weld path, resulting in a relatively narrower high-temperature region.

Fig. 6(b) shows the temperature distribution at 200 s, representing the end of the transient simulation. At this stage, heat has spread across the entire plate and decreased in magnitude due to cooling. Compared to sample 1#, the region that previously experienced high temperatures at 135 A appears more limited, and the cooling process seems to occur more rapidly.

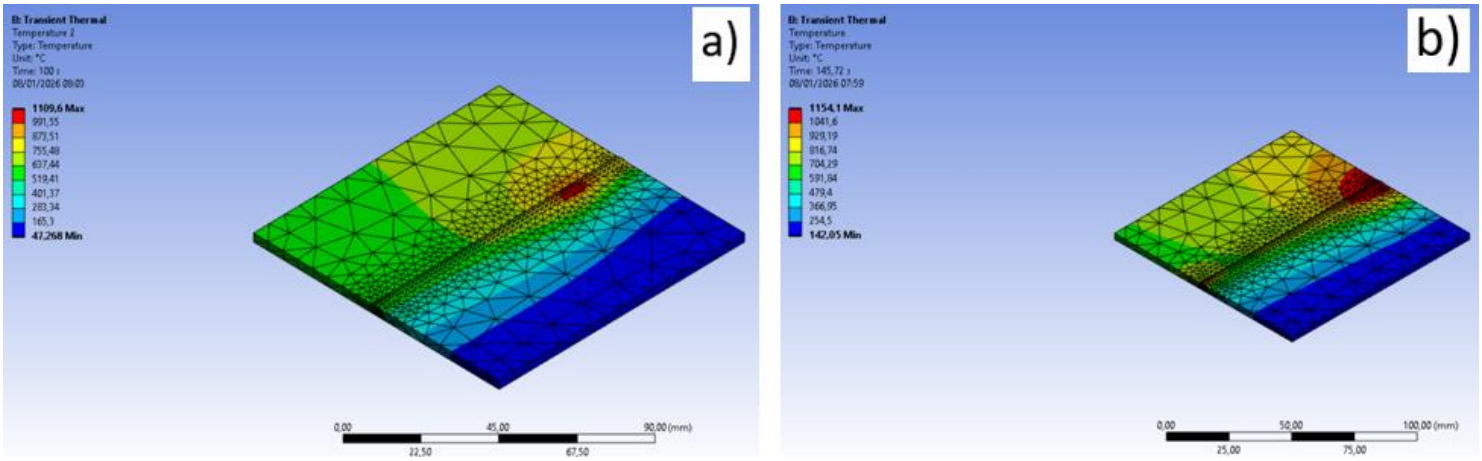

Fig. 6. (a) Temperature distribution at t = 100 s. (b) Temperature distribution at the end of welding (200 s).

The thermal trace along the weld line remains visible; however, the area corresponding to intermediate temperatures (yellow–green region) is smaller than in sample 1#. This indicates that the exposure to high temperatures occurs over a relatively shorter duration.

Fig. 7 shows that the weld metal reaches the highest temperature, with a peak of approximately ±2200°C occurring around 80–90 s, followed by a decrease and then a gradual increase. This indicates that the highest energy concentration occurs within the fusion zone. The HAZ Cu reaches a maximum temperature of approximately ±1500°C, exhibiting a rapid heating response but remaining lower than that of the weld metal. This behavior reflects the high thermal conductivity of Cu, which allows heat to be dissipated quickly. In contrast, the HAZ SS316L shows the lowest maximum temperature, around ±650–700°C, with a slower temperature increase.

The significant differences among the three curves indicate the presence of a steep thermal gradient in the joint region at a welding current of 135 A. This confirms the dominant heat concentration in the weld metal and the distinct thermal responses between the Cu and SS316L sides during dissimilar metal welding.

To evaluate the temperature distribution during the welding process for sample 3# at a welding current of 150 A, numerical simulations were conducted as shown in Fig. 8 and Fig. 9.

Fig. 8(a) presents the temperature distribution at t = 50 s, where the maximum temperature reaches 791.41°C and the minimum temperature is approximately 25.477°C. At this stage, the red–orange region remains relatively narrow and concentrated along the weld path. The lateral heat spread is still limited, and a sharp thermal gradient is observed from the weld line toward the SS316L side, which appears in blue. This indicates that at 50 s the system is still in the active heating phase, where the heat source moves rapidly and the supplied energy has not yet diffused extensively across the plate.

Fig. 8(b) shows the temperature distribution at t = 100 s, representing the final stage of welding for this case. The maximum

temperature increases to 1048.1°C, while the minimum temperature rises to approximately 51.898°C. The high-temperature zone becomes more developed compared to t = 50 s; however, it remains localized around the weld path. The transition from red to green and blue occurs within a relatively short distance, indicating a high thermal gradient. Heat spread toward the Cu side remains more pronounced than toward the SS316L side, consistent with the higher thermal conductivity of Cu.

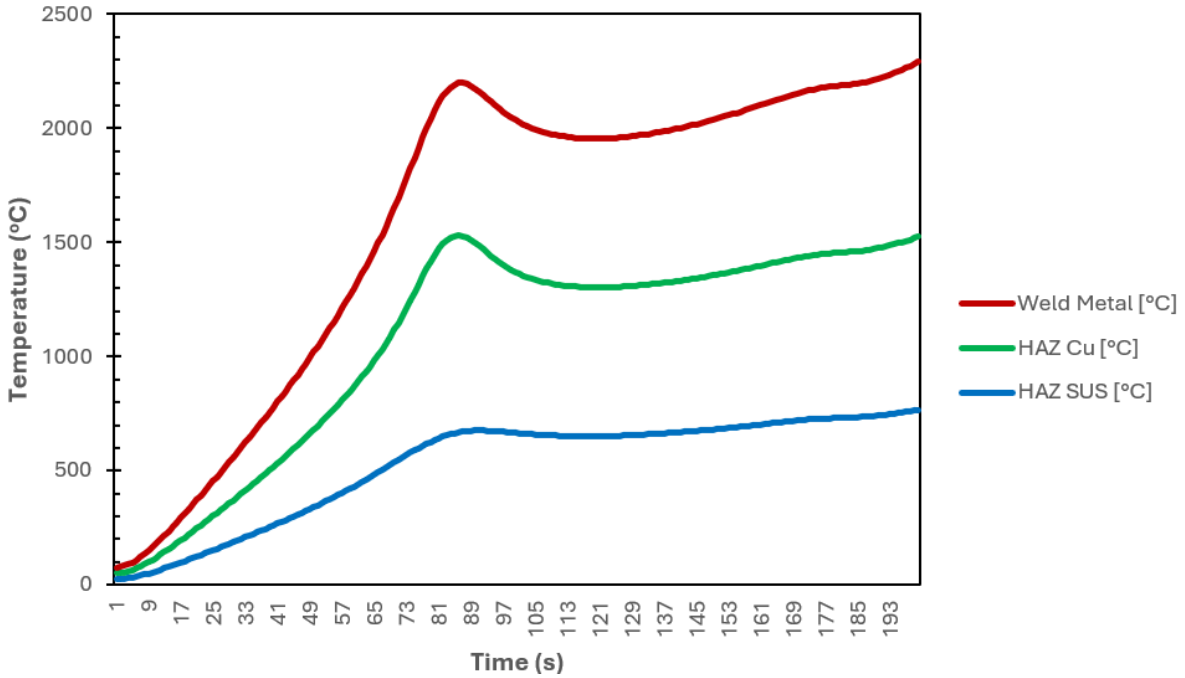

Fig. 7. Temperature distribution at the weld metal, Cu HAZ, and SS316L HAZ (135 A).

The difference in observation times (50 s and 100 s) between samples 1# and 2# compared to sample 3# is associated with the increased welding speed resulting from the higher current. With a faster moving heat source, the maximum heating phase occurs earlier, requiring representative thermal conditions to be evaluated at shorter time intervals. Overall, at 150 A, the temperature distribution exhibits a faster and more focused heating pattern, with a relatively narrow high-temperature zone despite the maximum temperature being sufficiently high to form a fusion zone.

Fig. 9 presents the temperature evolution over time at three different locations: weld metal, HAZ Cu, and HAZ SS316L. In general, all curves exhibit a progressive temperature increase from the beginning of the simulation, reaching a peak around 85–95 s, followed by a decrease and subsequent stabilization.

In the weld metal region (red curve), the temperature rises most rapidly and reaches a peak of approximately ±780°C at around 90 s. After reaching the peak, the temperature decreases to about 560°C and then gradually increases again toward the end of the observation period. This pattern indicates that the observation point experiences maximum heating when the heat source is located nearby, followed by a cooling phase as the heat source moves away.

In the HAZ Cu region (green curve), the maximum temperature reaches approximately ±600°C. The temperature increase occurs relatively quickly and follows a similar trend to the weld metal curve, although with a lower peak value. This behavior reflects that the Cu side receives heat from the fusion zone but rapidly redistributes it due to its high thermal conductivity.

Meanwhile, the HAZ SS316L region (blue curve) shows the lowest maximum temperature, around ±560°C, with a slower temperature rise compared to HAZ Cu. This difference indicates that the SS side experiences more limited heating, and the thermal gradient between the weld metal and the HAZ SS region is relatively significant.

Overall, at a welding current of 150 A, the maximum temperature is lower than that observed at 135 A in the previous case; however, the curves exhibit a faster rise and fall pattern. This suggests that the heating process occurs over a shorter duration and that the heat distribution is more localized. The temperature gradient between the weld metal and both HAZ regions remains clearly visible, reflecting the characteristic behavior of dissimilar Cu–SS316L welding.

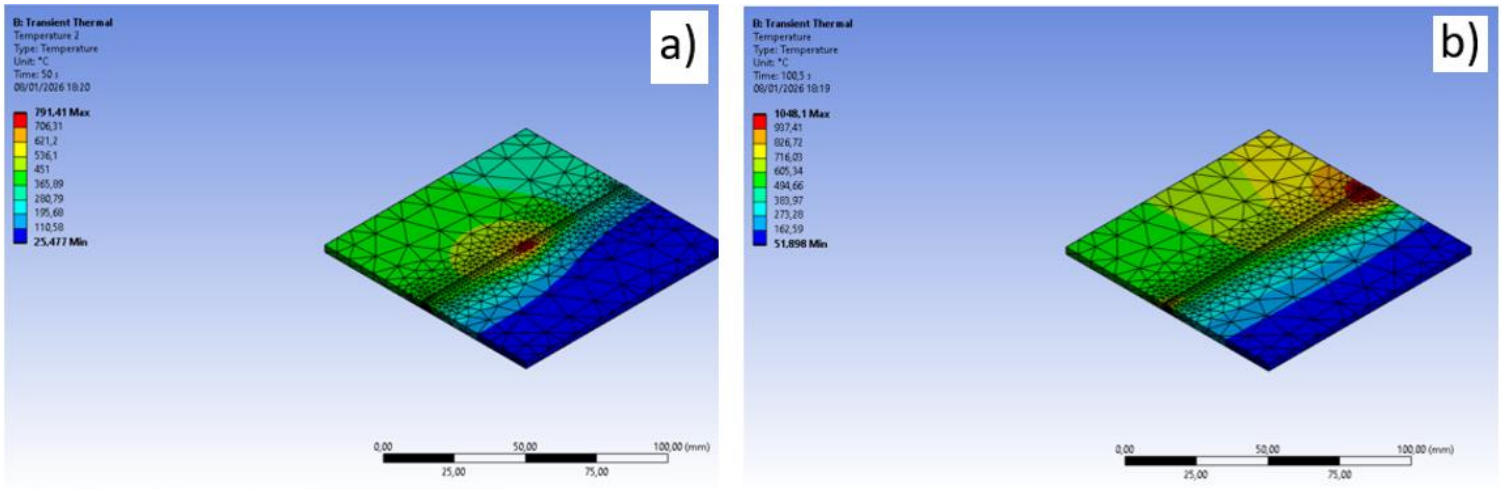

Fig. 8. (a) Temperature distribution at t = 50 s. (b) Temperature distribution at the end of welding (100 s).

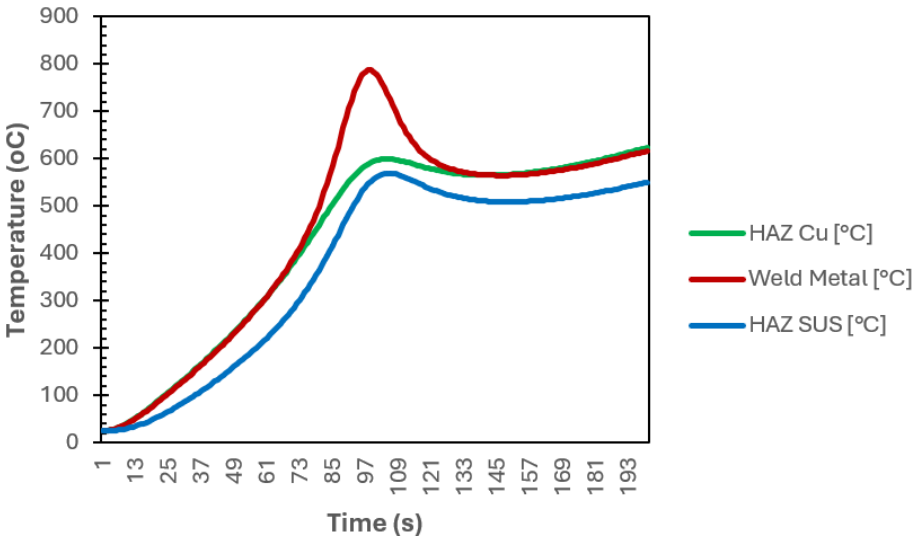

Fig. 9. Temperature distribution at the weld metal, Cu HAZ, and SS316L HAZ (150 A).

4 Conclusions

This study investigated the effect of welding current (120 A, 135 A, and 150 A) on the thermal distribution and macrostructural characteristics of TIG-welded Cu/SS316L dissimilar joints using ERCuSi-A filler through an integrated experimental and finite element approach. The results demonstrate that welding current strongly governs weld bead geometry and penetration behavior due to asymmetric thermal distribution arising from the large thermal conductivity mismatch between Cu and SS316L. At 120 A, rapid heat dissipation in copper limited penetration, while at 150 A, deeper penetration into SS316L was achieved but with a more localized heating cycle and concentrated fusion region. The 135 A condition provided the most balanced thermal response, producing a uniform fusion profile and stable penetration on both materials. Numerical simulations confirmed that heat dissipates rapidly into the Cu side and concentrates in the SS316L region, directly influencing weld morphology and fusion characteristics. The strong agreement between simulated thermal fields and experimental macrographs confirms that weld geometry is fundamentally governed by thermal distribution behavior. Therefore, 135 A is identified as the optimal welding current for achieving balanced fusion and controlled penetration in Cu/SS316L dissimilar joints, making it suitable for heat-transfer and cooling system applications.

Acknowledgments

The first author sincerely acknowledges the support provided by the National Research and Innovation Agency (BRIN) through the "Degree by Research Program" under contract number 27/II/HK/2024. Furthermore, the authors extend their deepest appreciation to Diponegoro University and the PRTRN BRIN management team for their invaluable contributions toward the successful completion of this research. In addition, the authors would like to thank the financial support provided by the Ministry of Higher Education, Science, and Technology under the Regular Fundamental Research Scheme, through grant numbers 037/C3/DT.05.00/PL/2025 and 508/C3/DT.05.00/PL-PNL/2025.

References

[1] J. Andersson, "Welding metallurgy and weldability of superalloys," *Metals*, vol. 10, no. 1. MDPI, p. 143, 2020.

[2] K. Kumar, C. S. Kumar, M. Masanta, and S. Pradhan, "A review on TIG welding technology variants and its effect on weld geometry," *Mater. Today Proc.*, vol. 50, pp. 999–1004, 2022.

[3] L. I. Markashova, V. D. Poznyakov, E. N. Berdnikova, A. A. Gajvoronsky, and T. A. Alekseenko, "Effect of structural factors on mechanical properties and crack resistance of welded joints of metals, alloys and composite materials," *Pat. Weld. J*, vol. 6, no. 7, pp. 22–28, 2014.

[4] N. Yadaiah and S. Bag, "Effect of heat source parameters in thermal and mechanical analysis of linear GTA welding process," *ISIJ Int.*, vol. 52, no. 11, pp. 2069–2075, 2012.

[5] S. Singh, "Analysis of various defects involved in welding metallurgy," *Int. J. Pure Appl. Math.*, vol. 120, no. 6, pp. 6267–6280, 2018.

[6] K. Antony and T. R. Rakeshnath, "Dissimilar laser welding of commercially pure copper and stainless steel 316L," *Mater. Today Proc.*, vol. 26, pp. 369–372, 2020.

[7] M. Li and S. J. Zinkle, "Physical and mechanical properties of copper and copper alloys," 2012.

[8] M. H. Kusuma, U. Setiorini, T. A. R. Putri, G. A. R. Antariksawan, and M. Juarsa, "Effective thermal conductivity of U-shaped heat pipe," *IOP Conf. Ser. Mater. Sci. Eng.*, vol. 550, no. 1, p. 012004, Jul. 2019, doi: 10.1088/1757-899X/550/1/012004.

[9] T. Pasang *et al.*, "Microstructure and mechanical properties of welded additively manufactured stainless steels SS316L," *Met. Mater. Int.*, vol. 25, no. 5, pp. 1278–1286, 2019.

[10] B. Tomar and S. Shiva, "Microstructural and mechanical properties examination of SS316L-Cu functionally graded material fabricated by wire arc additive manufacturing," *CIRP J. Manuf. Sci. Technol.*, vol. 50, pp. 26–39, 2024.

[11] Y. Singla, "Mechanical Properties Study of Copper/Stainless Steel Dissimilar Weld Joints," *Mod. Approaches Mater. Sci.*, vol. 2, no. 4, pp. 271–273, 2020, doi: 10.32474/mams.2020.02.000144.

[12] Y. Poo-arporn *et al.*, "Gas tungsten arc welding of copper to stainless steel for ultra-high vacuum applications," *J. Mater. Process. Technol.*, vol. 277, p. 116490, 2020.

[13] A. R. Pavan, N. Chandrasekar, B. Arivazhagan, S. Kumar, and M. Vasudevan, "Study of arc characteristics using varying shielding gas and optimization of activated-tig welding technique for thick AISI 316L (N) plates," *CIRP J. Manuf. Sci. Technol.*, vol. 35, pp. 675–690, 2021.

[14] J. Singh, L. Thakur, and S. Angra, "Effect of argon flow rate and standoff distance on the microstructure and wear behaviour of WC-CoCr TIG cladding," in *Journal of Physics: Conference Series*, IOP Publishing, 2019, p. 12162.

[15] S. C. Moi, P. K. Pal, A. Bandyopadhyay, and R. Rudrapati, "Effect of Heat Input on the Mechanical and Metallurgical Characteristics of TIG Welded Joints.," *J. Mech. Eng.*, vol. 16, no. 2, 2019.

[16] Y. Xu *et al.*, "Correlation between the microstructure and corrosion behaviour of copper/316 L stainless-steel dissimilar-metal welded joints," *Corros. Sci.*, vol. 191, p. 109729, 2021.

[17] Y. Meng, X. Li, M. Gao, and X. Zeng, "Microstructures and mechanical properties of laser-arc hybrid welded dissimilar

pure copper to stainless steel," *Opt. Laser Technol.*, vol. 111, pp. 140–145, 2019.
[18] Q. Nguyen, A. Azadkhou, M. Akbari, A. Panjehpour, and A. Karimipour, "Experimental investigation of temperature field and fusion zone microstructure in dissimilar pulsed laser welding of austenitic stainless steel and copper," *J. Manuf. Process.*, vol. 56, pp. 206–215, 2020.
[19] E. Zumelzu and C. Cabezas, "Study on welding such dissimilar materials as AISI 304 stainless steel and DHP copper in a sea-water environment. Influence of weld metals on corrosion," *J. Mater. Process. Technol.*, vol. 57, no. 3–4, pp. 249–252, 1996.
[20] P. Anbarasu, R. Yokeswaran, A. G. Antony, and S. Sivachandran, "Investigation of filler material influence on hardness of TIG welded joints," *Mater. Today Proc.*, vol. 21, pp. 964–967, 2020.
[21] N. Jeyaprakash, A. Haile, and M. Arunprasath, "The parameters and equipments used in TIG welding: A review," *Int. J. Eng. Sci.*, vol. 4, no. 2, pp. 11–20, 2015.
[22] E. S. V Marques, F. J. G. Silva, and A. B. Pereira, "Comparison of finite element methods in fusion welding processes—A review," *Metals (Basel).*, vol. 10, no. 1, p. 75, 2020.
[23] C. E. Etin-osa and J. I. Achebo, "Analysis of optimum butt welded joint for mild steel components using FEM (ANSYS)," *Am. J. Nav. Archit. Mar. Eng.*, vol. 2, no. 3, pp. 61–70, 2017.
[24] H. Arora, K. M. Basha, D. N. Abhishek, and B. Devesh, "Welding simulation of circumferential weld joint using TIG welding process," *Mater. Today Proc.*, vol. 50, pp. 923–929, 2022.
[25] I. A. Bataev, "Structure of explosively welded materials: experimental study and numerical simulation," *Met. Work. Mater. Sci*, vol. 77, pp. 55–67, 2017.
[26] A. Azwinur, M. H. Kusuma, U. Usman, and S. Dharma, "Effects of Heat Input on Mechanical Properties, Microstructures and Thermal Conductivity of Copper Alloy in Gas Tungsten Arc Welding Technology," *Adv. Sci. Technol. Res. J.*, vol. 16, no. 6, 2025, [Online]. Available: https://www.astrj.com/Effects-of-Heat-Input-on-Mechanical-Properties-Microstructures-and-Thermal-Conductivity,203367,0,1.html